

Using peak distribution of the cosmic microwave background for MAP and Planck data analysis: formalism and simulations

C. Hernández-Monteagudo¹

*Física Teórica. Facultad de Ciencias.
Universidad de Salamanca, 37008 Spain.
e-mail: chm@orion.usal.es*

A. Kashlinsky

*SSAI, Code 685, Goddard Space Flight Center, Greenbelt, MD 20771
e-mail: kashlinsky@stars.gsfc.nasa.gov*

F. Atrio-Barandela

*Física Teórica. Facultad de Ciencias.
Universidad de Salamanca, 37008 Spain.
e-mail: atrio@orion.usal.es*

ABSTRACT

We implement and further refine the recently proposed method (Kashlinsky, Hernández-Monteagudo & Atrio-Barandela, 2001 - KHA) for time-efficient and accurate extraction of the power spectrum from future cosmic microwave background (CMB) maps. The method is based on the clustering properties of peaks and troughs of the Gaussian CMB sky. The procedure takes only $\frac{1}{2}[f(\nu)]^2 N^2$ steps where $f(\nu)$ is the fraction of pixels with $|\delta T| \geq \nu$ standard deviations in the map of N pixels. We use the new statistic introduced in KHA, ξ_ν , which characterizes spatial clustering of the CMB sky peaks of progressively increasing thresholds. In this way the tiny fraction of the remaining pixels (peaks and troughs) contains the required information on the CMB power spectrum of the entire map. The threshold ν is the only parameter that determines the accuracy of the final spectrum. We performed detailed numerical simulations of MAP and Planck CMB sky data including cosmological signal, inhomogeneous noise and foreground residuals. In all cases we find that the method accurately recovers the power spectrum out to the Nyquist scale of the experiment channel. We show how the error bars scale with ν and how one can decide between accuracy and speed. We determine very accurately the CMB power spectrum from the upcoming CMB maps in only $\sim (10^{-5} - 10^{-3}) \times N^2$ operations, which is significantly faster than the current methods. For MAP parameters the KHA method would work for $\nu = 2 - 2.5$; for Planck it would work for threshold as high as $\nu = 2.5 - 3$.

Subject headings: cosmology - cosmic microwave background - methods: numerical

¹Current address: Max-Planck-Institut für Astrophysik, Postfach 1317. D-85741 Garching, Germany

1. Introduction.

The sub-degree structure of the CMB probes linear scales that were inside the horizon at the last scattering epoch. The CMB fluctuations on these scales carry a signature of causal processes during the last scattering and thereby provide a very important constraint on the physics of the early Universe and the models for structure formation. The most popular of these models is the cold dark matter (CDM) set of models based on the inflationary paradigm for the evolution of the early Universe. The models are very appealing, not only because of their relative simplicity, but also because they provide a clear-cut set of predictions that can be verified by observations. One (and perhaps the most critical) of these predictions is the sub-degree structure of the CMB anisotropies. In the framework of CDM models with adiabatic density fluctuations the structure of the CMB power spectrum reflects the linear physics of sound waves and initial density perturbations. While on scales outside the horizon at de-coupling the CMB field preserves the initial power spectrum, on sub-degree scales the interaction between the photon fluid and matter leads to a series of acoustic peaks. The relative height, width and spacing of these peaks depend on a final set of the cosmological parameters ($\Omega_{\text{total}}, \Omega_{\Lambda}, \Omega_{\text{baryon}}, h$) and also serve to validate the cosmological CDM paradigm (see Hu & Dodelson 2002 for a recent review). It is then important to measure the sub-degree structure of the CMB with high accuracy as is being done with the current ground-based (e.g. DASI), balloon (BOOMERANG, MAXIMA, TOP-HAT) and space-borne experiments (MAP).

A major challenge to understanding future CMB measurements is to find an efficient algorithm that can reduce these enormous datasets: $N \simeq 10^5$ pixels in balloon experiments, $\simeq 3 \times 10^6$ for MAP, to $\simeq 5 \times 10^7$ for the Planck HFI data. (For comparison the COBE DMR data analysis was based on only 4,144 pixels). Traditional methods require inverting the covariance matrix and need $\sim N^3$ operations making them unfeasable for the current generation of computers. Thus alternatives have been developed for estimating the CMB multipoles from Gaussian sky maps: Tegmark (1997) proposed a least variance method that yields C_l 's directly from the temperature map, while Oh, Spergel & Hinshaw (1999) solve the maximal likelihood iteratively. Both approaches require $O(N^2)$ operations. Bond, Jaffe & Knox (2000) and

Wandelt, Hivon & Górski (2001) concentrate on the statistics of C_l 's, once the temperature MAP has been Fourier transformed. Hivon et al. (2002) studied the likelihood of the power spectrum as obtained by direct Fast Fourier Transform of the available portion of the sky. Though it requires $O(N^{3/2} \ln N)$ operations, the accuracy of their results depends on the fraction of the sky covered. A different approach consists in computing the correlation function directly from the data, procedure that takes $O(N^2)$ operations. Smoot et al. (1992) used this type of analysis for the first year release of the COBE data. More recently, Szapudi et al. (2001a,b) have developed it for megapixel CMB data sets.

Recently we proposed a new method to compute the CMB power spectrum in a fast and accurate manner (Kashlinsky, Hernández-Monteagudo & Atrio-Barandela, 2001, hereafter KHA). The method exploits Gaussian properties of the CMB and noise fields and uses high peaks (and troughs) of the CMB field whose abundance is much smaller than the total number of pixels, N , and whose correlation properties are strongly amplified in a way that depends on the underlying power spectrum. *This simultaneously achieves two important goals: reducing the number of computational steps for analysis and the high accuracy of the measured parameters.* KHA have shown that the tiny fraction of the remaining pixels (peaks and troughs) contains the required information on the CMB power spectrum of the entire map.

In this paper we present detailed numerical simulations with the application of the KHA method to MAP and Planck datasets in the presence of realistic noise and Galactic foregrounds. We show that with this method we can determine the CMB power spectrum outside the beam ($l \simeq 640$ for MAP and higher for Planck) in only $< 10^{-3} N^2$ operations with an uncertainty comparable with any other existing method. In practice, this means that a CMB power spectrum computation that takes many months of CPU time with previous methods, requiring $O(N^2)$ operations, can be done in only a few hours CPU time with our method. For both MAP and Planck parameters the KHA method is also faster than the direct computation of the CMB power spectrum in $O(N^{3/2} \log N) \sim N^{1.61}$ steps.

The structure of this paper is as follows: In Sec. 2 we review the KHA formalism and in Sec. 3 we discuss its numerical implementation. Sec. 4 deals with application of the method to both idealized and

realistic MAP CMB maps. We show there that the method is rather immune to noise inhomogeneities and non-Gaussian features of Galactic foregrounds. Sec. 5 follows with results for application of the KHA method to Planck data and we conclude in Sec. 6.

2. Mathematical formalism: an overview

In this section we briefly summarize the KHA formalism; more details are given in the KHA paper. Peaks are much fewer in number than pixels, but they are strongly clustered. Therefore KHA considered a new statistic describing their angular clustering - the 2-point angular correlation function ξ in analogy to the galaxy correlation function (Peebles 1980), i.e. the excess probability over the Poisson process of finding two peaks at a given separation angle. This correlation function is strongly amplified over the scales of interest ($<10^\circ$). The value of ξ for a given peak threshold $|\delta T| \geq \nu\sigma$ would be uniquely related to the correlation function of the temperature field $C(\theta) = \langle \delta T(\vec{x}) \delta T(\vec{x} + \vec{\theta}) \rangle$. The measurement of $\xi(\theta)$ can then be uniquely inverted to obtain the underlying $C(\theta)$ and its Fourier transform, the power spectrum C_l ; they are related via $C(\theta) = \sum (2l+1) C_l P_l(\cos \theta) / 4\pi$. This can be achieved in just $[f(\nu)]^2 N^2$ operations, where $f(\nu) = \text{erfc}(\nu/\sqrt{2})$ is the fraction of pixels with $|\delta T| \geq \nu\sigma$ and is e.g. 4.5–1% for $\nu=2–2.5$.

The CMB sky is expected to be highly Gaussian and this property, eq. (1) below, is also widely used in standard maximum likelihood methods. For a Gaussian ensemble of N data points (e.g. pixels) describing the CMB data $\delta \equiv T - \langle T \rangle$ one will find a fraction $f(\nu) = \text{erfc}(\nu/\sqrt{2})$ with $|\delta| \geq \nu\sigma$, where $\sigma^2 = \langle \delta^2 \rangle$ is the variance of the field and erfc is the complementary error function. The fraction of peaks, $f(\nu)$, is a rapidly decreasing function for $\nu \sim 1$ and is e.g. $f(\nu) = (4.5, 1, 0.1) \times 10^{-2}$ for $\nu = (2, 2.5, 3)$ respectively. The joint probability density of finding two pixels within $d\delta_{1,2}$ of $\delta_{1,2}$ and separated by the angular distance θ is given by the bivariate Gaussian:

$$p(\delta_1, \delta_2) = \frac{1}{2\pi\sqrt{\|\mathbf{C}\|}} \exp\left(-\frac{1}{2}\boldsymbol{\delta} \cdot \mathbf{C}^{-1} \cdot \boldsymbol{\delta}\right) \\ = \int_{-\infty}^{\infty} \int_{-\infty}^{\infty} \frac{d^2\mathbf{q}}{(2\pi)^2} \exp(-i\mathbf{q} \cdot \boldsymbol{\delta}) \exp\left(-\frac{1}{2}\mathbf{q} \cdot \mathbf{C} \cdot \mathbf{q}\right) \quad (1)$$

where \mathbf{C} is the covariance matrix of the temperature field. We model the covariance matrix in eq. (1) as

$$C(\theta) = C_0 \delta_{ij} + C(\theta_{ij})(1 - \delta_{ij}) \quad (2)$$

where δ_{ij} is the Kronecker delta and $C_0 \equiv C(0) + \langle r^2 \rangle$; r is the noise contribution. The total dispersion of the

temperature field is then $\sigma = \sqrt{C(0) + \langle r^2 \rangle}$. This expression assumes for now that the noise is white and homogeneous; generalization to inhomogeneous noise with pixel dependent noise variance is given in Sec. 4.2.

The distribution of peaks of a Gaussian field is strongly clustered (Rice 1954, Kaiser 1984, Jensen & Szalay 1986, Bardeen et al 1986, Kashlinsky 1987). Their angular clustering can be characterized by the 2-point correlation function, ξ , describing the excess probability of finding two events at the given separation. I.e. if the probability of simultaneously finding two temperature excursions with $|\delta T| \geq \nu\sigma$ in small solid angles $dw_{1,2}$ is $dP_{12} \propto (1 + \xi)dw_1 dw_2$ then the correlation function of such regions will be:

$$\xi_\nu(\theta) = \frac{2 \int_{\nu\sigma}^{\infty} \int_{\nu\sigma}^{\infty} [p(\delta_1, \delta_2) + p(-\delta_1, \delta_2)] d\delta_1 d\delta_2}{[2 \int_{\nu\sigma}^{\infty} p(\delta) d\delta]^2} - 1 \\ = A_\nu \left(\frac{C}{C_0} \right) \quad (3)$$

where A_ν was evaluated in detail in KHA, and it was found to be:

$$A_\nu(x) = \frac{1}{H_{-1}^2(\frac{\nu}{\sqrt{2}})} \sum_{k=1}^{\infty} \frac{x^{2k}}{2^{2k}(2k)!} H_{2k-1}^2(\frac{\nu}{\sqrt{2}}) \quad (4)$$

Here $H_n(x) = (-1)^n \exp(x^2) d^n/dx^n \exp(-x^2)$ is the Hermite polynomial and $H_{-1}(x) \equiv \frac{\sqrt{\pi}}{2} \exp(x^2) \text{erfc}(x)$. At each angular scale the value of ξ_ν for every ν is determined uniquely by C at the same angular scale.

Fig. (1) shows two realizations of two different cosmological models: left panels correspond to an $(\Omega_{total} = 1, \Omega_\Lambda = 0)$ model with $n = 1$ and $\Omega_b h^2 = 0.03$ for the MAP experiment 90GHz channel parameters. Right panels show an $(\Omega_{total} = 1, \Omega_\Lambda = 0.3)$ universe with $n = 1$ and $\Omega_b h^2 = 0.01$ under PLANCK resolution. Pixels with $|\delta T| \geq \nu\sqrt{C_0}$, with $\nu=2.25$ (top) and 1.75 (bottom) are shown. The clustering of peaks/troughs is very prominent especially on small scales.

It is important to emphasize that in the limit of the entire map ($\nu=0$) our statistic is $\xi_\nu=0$ and our method becomes meaningless; the new statistic has meaning only for sufficiently high ν . One should distinguish between the 2-point correlation function, ξ_ν , we directly determine from the maps, and the commonly used statistics in CMB studies, the temperature correlation function, C . We also note in passing, in order to avoid confusion, that the KHA methods

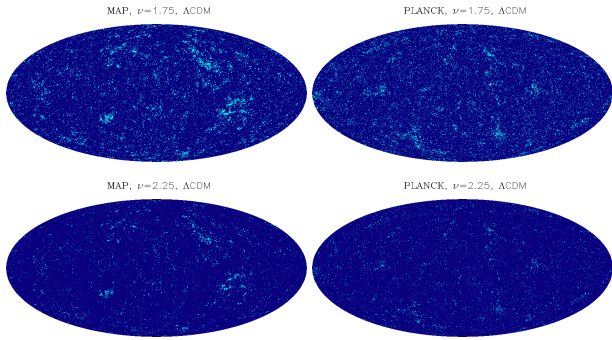


Fig. 1.— Two different realizations of the CMB sky as seen by the FWHM=0.21° MAP and Planck 217 GHz channels.

works with the distribution of peaks and troughs, i.e. hot and cold spots, not the extrema of the CMB field.

The terms with $k > 1$ contribute significantly to eq. (4) and there would be quasi- ($\xi_\nu \sim 1$) to non-linear ($\xi_\nu > 1$), and easy to detect, clustering of high peaks out to the angular scale where $C(\theta)$ drops to only $\lesssim 0.1$ of its maximal value at zero-lag. This covers the angular scales of interest for determining the sub-horizon structure at the last scattering. Because the uncertainty in measuring ξ_ν is $\sim N_{\text{pairs}}^{-1/2}$ (Peebles 1980), the value of ξ_ν can be determined quite accurately in the non-linear to quasi-linear regime. At the same time, over this range of scales the amplitude of ξ_ν changes very rapidly with C (see Fig. 1 of KHA) making possible a stable inversion procedure to obtain $C(\theta)$ from a given ξ_ν .

KHA thus suggested the following procedure to determine the power spectrum of CMB in only $\simeq f^2(\nu)N^2 \ll N^2$ operations:

1. Determine the variance of the CMB temperature, C_0 , from the data in N operations;
2. Choose sufficiently high value of ν when $f(\nu)$ is small but at the same time enough pixels are left in the map for robust measurement of $\xi_\nu(\theta)$;
3. Determine $\xi_\nu(\theta)$ in $[f(\nu)]^2 N^2$ operations.
4. Finally, given the fixed values of (C_0, ν) solve equation $A_\nu(C/C_0) = \xi_\nu(\theta)$ to obtain $C(\theta)$ and from it C_l .

Formally speaking this procedure would require $\frac{1}{2}[f(\nu)]^2 N^2$ operations because of the symmetry in counting pairs. For simplicity we will be referring to

this as $O(f^2 N^2)$ method implying a gain factor of $[f(\nu)]^2$ compared to other $O(N^2)$ methods.

3. Numerical implementation

The CMB sky was simulated for CDM models with Gaussian distributed multipoles. The spectrum of the CMB sky for the given CDM model was obtained by CMBFAST (Seljak & Zaldarriaga, 1996). To this we added Gaussian white noise and a foregrounds model as described in Sec. 4.

Maps of the CMB sky were generated using the hierarchical equal area isolatitude pixelization of the celestial sphere implemented in HEALPix¹. Pixels have equal area and are arranged in “constant latitude rings”. Maps can be constructed with varying resolution, the number of pixels given by $N = 12 \times N_{\text{side}}^2$, being N_{side} the number of times in which each side of a pixel will be divided in two, starting from a given initial configuration. For a value of N_{side} of 512, one generates a map of 3,145,728 pixels of size of seven arcminutes. This configuration is adopted by the MAP team for the future data release, and was the choice for our simulations of this experiment. For PLANCK, $N_{\text{side}} = 1024$ or 12,582,912 pixels of 3.5 arcminutes size.

For MAP, we performed two type of simulations including: (1) cosmological signal plus white noise, and (2) cosmological signal, foregrounds and inhomogeneous white noise. For Planck, we only run simulations with homogeneous noise, but we note that because of the smallness of the Planck noise this approximation is quite adequate. We chose three different thresholds: $\nu = 2.0, 2.27, 2.525$ for MAP and $\nu = 2.55, 2.78, 3.0$ for Planck. For each threshold this selects, on average, $f(\nu)N$ peaks from the map and these particular values were chosen to have double the average number of pixels with decreasing threshold. Due to the PLANCK higher resolution the above thresholds select the same number of pixels in both experiments and we can analyze the effect of pixel number on the accuracy of our method.

From the peak spatial distribution, $\xi_\nu(\theta)$ was computed on a grid of 31,415 equally spaced bins. Fig. (2) shows $\xi_\nu(\theta)$ for the SCDM model. The solid line corresponds to the theoretical prediction and the dashed line is a smooth average obtained from the data. The agreement is very good out to $\theta \sim 10^\circ$, allowing an

¹HEALPix’s URL site: (<http://www.eso.org/science/healpix>)

accurate reconstruction of the power spectrum in the range of interest: $l \gtrsim 30$.

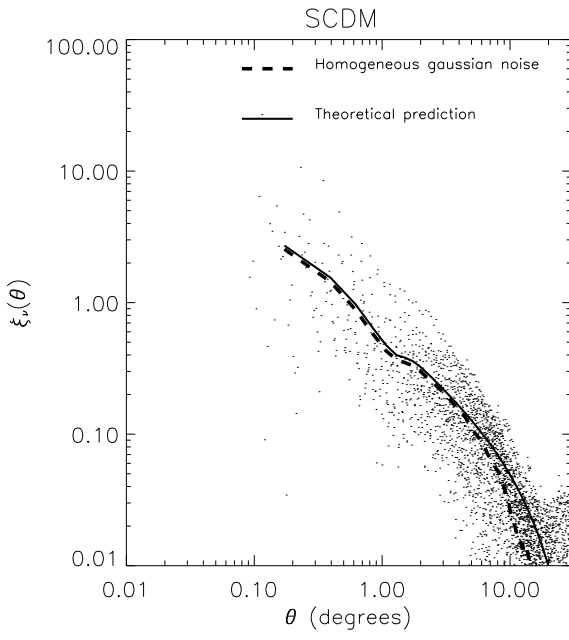


Fig. 2.— The 2-point correlation function ξ_ν for $\nu = 2$ for the SCDM model from a single realization of MAP 90GHz channel. The solid line corresponds to the theoretical estimate given by eq. (3). Dots are estimates of ξ_2 in 31,415 angular bins from $\theta = 0^\circ$ to 180° . The dashed line is the result of filtering the raw data with a Gaussian of $\sigma = 4'$ at the roots of the Legendre polynomial of $l_{\max} = 800$ order.

After estimating $\xi_\nu(\theta)$ we invert eq. (3) to obtain $C(\theta)$ for the map. The power spectrum is obtained by means of Gauss-Legendre quadratures as:

$$C_l = 2\pi \int_0^\pi d\theta \sin \theta C(\theta) P_l(\cos \theta). \quad (5)$$

An accurate computation of this integral requires the evaluation of $C(\theta)$ at the roots of the Legendre polynomial out to a maximum order l_{\max} (Press et al 1992) and this property was used by Szapudi et al (2001a,b) and KHA. The value of l_{\max} was chosen as a compromise between the beam scale, so high order multipoles are calculated, and the pixel angular scale to prevent the first root of the Legendre polynomial from being within the pixel size, where there is no

information on $\xi_\nu(\theta)$. Prior to all calculations, $\xi_\nu(\theta)$ was smoothed using a narrow Gaussian centered on the roots of the Legendre polynomials.

At $\theta \gtrsim 10^\circ - 20^\circ$ the value of $\xi(\theta)$ is small and its determination becomes dominated by shot noise. Hence, we restrict the analysis to $\theta < 10^\circ - 20^\circ$ by introducing a taper function that cuts out the contribution of the correlation function for $\theta \gtrsim 10^\circ$. This leads to the following: (a) we will not recover very accurately multipoles below $l \simeq 30$ and (b) it introduces additional correlations among the different C'_l 's. The first limitation is irrelevant, since one can always degrade the map to smaller resolution and apply standard techniques to recover the power spectrum at $l \leq 20 - 40$. The second limitation is common to all methods that compute the power spectrum by means of the correlation function or in the presence of Galactic (and other) cut.

In our case, as in the case of any computation involving tapering (cf. Szapudi et al 2001a) with $C(\theta) = F(\theta)C_{\text{intrinsic}}$, the recovered multipoles are related to the intrinsic multipoles via:

$$C_l = \sum_{l'} C_{l'}^{\text{intrinsic}} \mathcal{F}_{l-l'} \quad (6)$$

where \mathcal{F}_l is the Legendre transform of the tapering function F . This introduces extra correlations between the multipoles.

Fig. (3) shows the Legendre transform of the tapering function as function of $\Delta l \equiv l - l'$ for Gaussian and top-hat tapering. The advantage of Gaussian tapering is quite obvious as it leads to significantly less prominent side-lobes. Hence we adopted the Gaussian tapering in the discussion below. As the figure shows it would lead to FWHM correlation width of only $\Delta l \sim$ a few for tapering angles $\lesssim 10^\circ$.

4. Application to MAP

The MAP satellite² was launched on June 30, 2001 for a 27 month mission - 3 months en route to and 24 months of observing time at L2. By design the observatory will scan the full sky every six months. MAP will observe the full sky at 5 frequency bands: 22, 30, 40, 60, and 90 GHz. The beam response at each band is approximately Gaussian with a FWHM resolution of 0.93, 0.68, 0.53, 0.35, and $< 0.23^\circ$, respectively, at each frequency. The sky maps based

²(<http://map.gsfc.nasa.gov>)

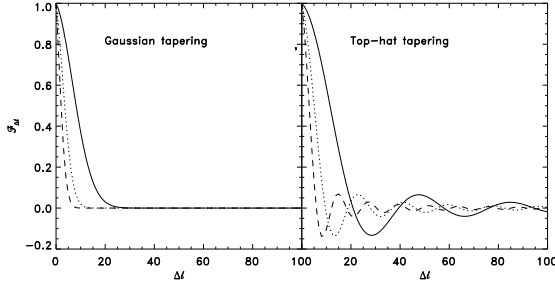


Fig. 3.— Legendre transform of the tapering function (eq. 6) plotted vs $\Delta\ell = l - l'$. Left panel corresponds to Gaussian tapering, $F(\theta) \propto \exp(-\theta^2/\theta_t^2)$ and the right panel to the top hat tapering, $F(\theta) = 1$ for $\theta \leq \theta_t$ and zero otherwise. Dashed, dotted and solid lines correspond to $\theta_t = 18^\circ, 12^\circ, 8^\circ$ respectively.

on the full two-years of data are expected to have an *rms* noise of $\simeq 35 \mu\text{K}$ per $0.3^\circ \times 0.3^\circ$ pixel. By design, the noise will be essentially uncorrelated from pixel to pixel and it is expected to be highly Gaussian (Hinshaw 2000). Due to the sky scanning strategy, the noise will be reasonably uniform across the sky, except the small regions near the ecliptic poles and at ecliptic latitude $\sim 45^\circ$ where the sensitivity will be somewhat higher. The MAP radiometers produce a raw temperature measurement that is the difference between two points on the sky $\sim 140^\circ$ apart. Since a given pixel i is observed with up to 1000 different pixels j , the covariance between any given pair of pixels (i, j) is much less than 1% of the variance of pixel i . The noise covariance in the final sky maps will, by design, be very nearly diagonal.

4.1. Homogeneous noise results

We first performed a set of 500 simulations including only cosmological signal and white noise. For each simulation we computed the correlation function and the power spectrum. Fig. (4) summarizes the results. In all plots, dotted lines display the input model, in this case SCDM with the parameters given above. In the top three panels, the thin solid lines represent the power spectra recovered from a single realization for the three different values of ν . In the bottom three panels we show the power spectrum averaged on bins of $\Delta\ell = 45$. The histogram shows the average C_l taken from the simulations, and the width corre-

sponds to the binning scale. The taper window used in these analyses was a Gaussian of FWHM of 13° . Our method recovers very accurately the radiation power spectrum out to the beam scale $l_{\text{beam}} \simeq 642$. At large scales or $l \lesssim 30$, our estimates deviate from the initial radiation power spectrum. This was expected, since tapering cuts out the correlation function on these scales.

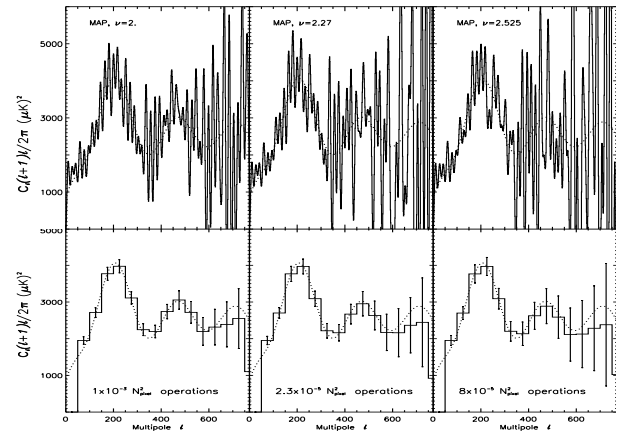


Fig. 4.— Radiation power spectrum for three different thresholds. Top panels show the power spectrum obtained from a single realization. Bottom panels show the band power estimates from 500 simulations, obtained by averaging in intervals of $\Delta\ell = 45$. In all plots, the dotted line represents the input model. The number of operations required to obtain the CMB power spectrum for the given ν is shown in the bottom panels.

Fig. 5 shows for all simulations the distribution of power spectrum amplitudes for three multipoles; more histogram examples were given in KHA. The distribution of multipoles is quasi-Gaussian as is to be expected at high l . Gaussian fits to the distributions are plotted with dashes. The width of the 68% confidence level from the histograms is practically coincident with the dispersion of the Gaussian fits and/or with the standard variance determined from the histogram, i.e. $\sigma_{C_l}^2 = \langle (C_l - \langle C_l \rangle)^2 \rangle$. At 95% confidence level the error will be approximately twice as large. One can clearly see that the width of the histogram increases with higher peak thresholds leading to less accurate determinations at high ν . The variance in this distribution was used in Fig. (4) to compute the

error bars.

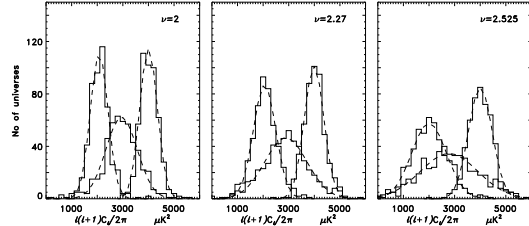


Fig. 5.— Histograms of multipoles at $l = 200, 350, 500$ obtained by the KHA method for 500 universes with SCDM model sky and a homogeneous MAP 90GHz channel noise. The dashed line shows a Gaussian fit.

Fig. (6) shows the map of the correlation matrix, $\mathcal{C}_{l,l'}$, among different multipoles given by:

$$\mathcal{C}_{l,l'} = \frac{\langle \delta C_l \delta C_{l'} \rangle}{\sqrt{\langle \delta C_l^2 \rangle \langle \delta C_{l'}^2 \rangle}}, \quad (7)$$

with $\delta C_l = C_l - \langle C_l \rangle$. The correlation coefficient matrix is highly diagonal with FWHM width $\Delta l \sim 10$ for $\theta_p = 18^\circ$ which compares favorably with other methods. The correlation drops to the floor level of $\Delta l \sim 5\%$ or $N_{\text{sim}}^{-1/2}$, determined by the finite number of simulations, at $\Delta l \sim 20$ almost independently of ν ; the scaling with θ_p follows that in Fig. 3. Outside the central diagonal strip the residual correlations are due to shot noise from the finite number of simulations. For consistency we repeated the analysis with only 125 simulations. The width of the diagonal remained the same, but the off diagonal terms grew by a factor of two, consistent with being due to shot noise.

Finally, we studied how the error bars on the band power estimates scaled with the number of peaks selected (i.e. with ν) and the width of the band power Δl . For completely uncorrelated multipoles one would expect the error bars on the band powers to scale with the size of the band Δl as $\sigma_{C_l} \sim (\Delta l)^{-1/2}$. At each value of l the cosmic variance error in the presence of white noise with variance $\langle r^2 \rangle$ is given by (Bond et al 2000):

$$\sigma_{CV} = \sqrt{\frac{2}{2l+1}} [C_l + \frac{4\pi \langle r^2 \rangle B_l^{-2}}{l_{\text{pix}}(l_{\text{pix}}+2)}] \quad (8)$$

where l_{pix} is the maximal multipole corresponding to the pixel size resolution and B_l is the beam function.

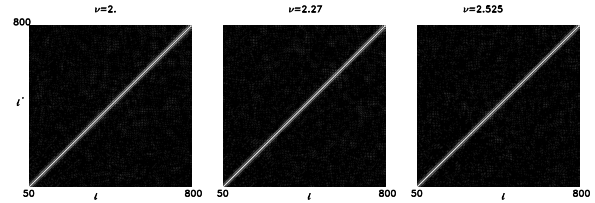


Fig. 6.— Maps of the cross-correlation matrix $\mathcal{C}_{l,l'}$ from eq. 7 shown up to $l = 800$. The maximal value shown correspond to unity correlation. The darkest shade corresponds to zero.

The left panel in Fig. (7) shows the ratio of the 68% error in the recovered multipole at $l = 200$ after band-averaging to the cosmic variance at the central l . One can see that the error starts decreasing as $1/\sqrt{\Delta l}$ after only $\Delta l \sim 5$ and practically coincides with the central l cosmic variance. The right panel of Fig. (7) shows the ratio vs the fractional bandwidth, $\Delta l/l$, for various values of the central multipole l and $\nu = 2$. The figure shows that for MAP parameters and $\nu = 2$ we reach the central l cosmic variance with the relative bandwidth of only a few percent. Note that even without bin-averaging the CMB spectrum, for $\nu = 2$ the method reaches the cosmic variance at $l = 200$ and increasing the uncertainty to only $\sim 2 - 2.5\sigma_{CV}$ at $l \sim 500 - 600$.

Fig. (8) shows σ_{C_l} at $l = 200, 300, 400, 500$ for the three threshold levels. Like before, smaller error bars correspond to the smaller threshold, i.e., to larger number of points. A power-law fit using all multipoles gives a power law behavior of the form $\sigma_{C_l} \propto N_{\text{peaks}}^\beta$, with $\beta = -0.4054 \pm 0.016$. These relations can be used to estimate the amplitude of the error bar attached to each multipole for a wide range of values of ν and Δl . In particular, it can be used to find what values of ν and Δl are necessary to achieve a given degree of accuracy in the power spectra.

We have shown that for a given experiment the accuracy of the recovered power spectrum depends mainly on one parameter: the peak threshold or number of pixels selected for the analysis. This accuracy can be further improved by changing the width of the multipole bins within which band power spectra are computed, but at the obvious expense of decreasing the number of independent estimates. The behavior

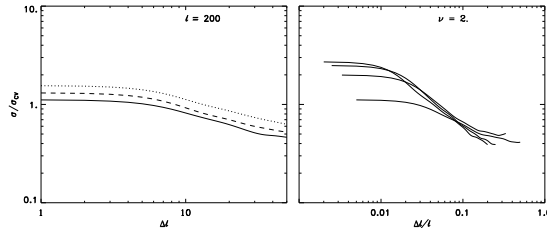


Fig. 7.— Left panel: The ratio of the 68% error in C_l at $l = 200$ to the cosmic variance at that l is plotted vs the bandwidth Δl . Solid line corresponds to $\nu = 2$, dashed line to $\nu = 2.27$ (half as many pixels as for $\nu = 2$), and dotted line to $\nu = 2.525$ (quarter of the pixels for $\nu = 2$).

Right panel: The quantity from the left panel is plotted vs the relative bandwidth $\Delta l/l$ for $\nu = 2$. The lines in order of increasing thickness (or from bottom to top at low $\Delta l/l$) correspond to $l = 200, 300, 400, 500$.

of the uncertainties in the recovered power spectra with respect to these two parameters is close to what one would expect for a poissonian process. This fact allows an *a priori* knowledge of the accuracy of the analysis, as it can be *gauged* by a proper choice of the peak threshold parameter ν .

4.2. Including foregrounds and realistic noise

We now generalize the method to include realistic foreground emission and inhomogeneous noise and will demonstrate that also in this case the KHA method gives accurate and robust estimate of the CMB power spectrum.

4.2.1. Foregrounds

Models of radio and dust emission based on all three COBE experiments and various balloon and ground-based CMB experiments all indicate that foreground galactic signals will not be a significant contaminant above a galactic latitude of 10° (except for isolated high-latitude clouds) (Finkbeiner, Davis & Schlegel 1999, de Oliveira-Costa et al. 2000). These models conservatively predict that galactic emission at 90 GHz will not exceed $100 \mu\text{K}$ above $b = 10^\circ$ and it should be possible to model and remove this contribution using the 5 frequencies of MAP data to within 10–20% or better (Hinshaw, private com-

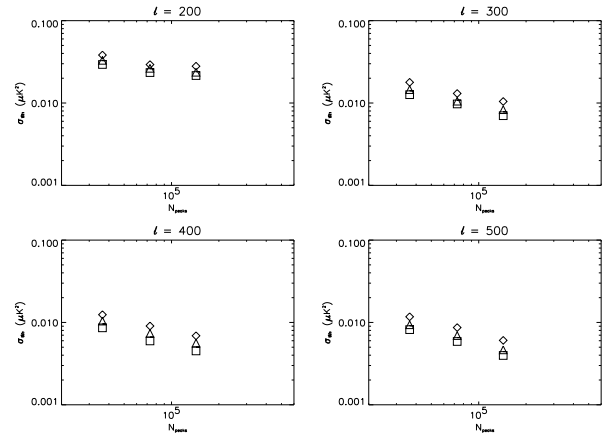


Fig. 8.— Band power error bars as a function of the number of pixels used to compute the radiation power spectrum for four values of l . Diamonds, triangles and squares correspond to $\Delta l = 30, 50, 70$, respectively.

munication, <http://map.gsfc.nasa.gov>). Adopting the fiducial number of 20% would already imply that foreground residuals above $b = 10^\circ$ are small compared to the intrinsic CMB temperature fluctuations associated with peaks ($\delta T \gtrsim 250 \mu\text{K}$ for $\nu = 2$).

To simulate the effect of foregrounds, we used simulated maps provided to us by G. Hinshaw of the MAP science team (private communication). These were produced by combining the Haslam 408 MHz map and the Schlegel, Finkbeiner & Davis (1988, hereafter SFD) IRAS/DIRBE 100 μm dust map. The Haslam map was used as the template for synchrotron emission and the SFD map as the template for dust and free-free. These maps were scaled to microwave frequencies using the COBE DMR-based fits of these templates (with 7 degree resolution). The frequency by frequency fit results are in Table 1 of Kogut et al. (1996). In detail, the Haslam map was scaled using a power law index $\alpha_{syn} = -3$. The SFD free-free map was scaled using $\alpha_{ff} = -2.15$ and the SFD dust model was scaled using an index $\alpha_{dust} = 2.0$. This model is known to over-predict the plane emission at DMR resolution, thus it is likely to be conservative. In the foreground maps, we did not include point sources. Sokasian, Gawiser & Smoot (1999) have compiled and analyzed the available extra-galactic point source data and have con-

cluded that such sources will contribute negligibly to the angular power spectrum at 90 GHz for $l < 800$.

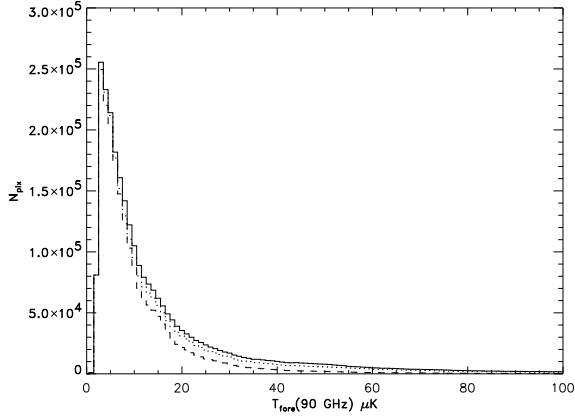


Fig. 9.— The histograms of the 90 GHz foreground emission with MAP resolution. Solid, dotted and dashed lines correspond to Galactic cut $b_{\text{cut}} = 5, 10, 20$ degrees, respectively.

Fig. (9) shows the histogram of foreground contributions to the MAP 90GHz channel for 3 values of Galactic cut: solid line is for $|b|_{\text{cut}} = 5^\circ$, dotted to 10° and dashes to $|b|_{\text{cut}} = 20^\circ$. For comparison at $\nu = 2$ the value CMB contribution to the remaining pixels will be $\sim 200\mu\text{K}$. This figure clearly indicates that the foregrounds are not likely to significantly affect the method.

4.2.2. Noise model

We input the noise using a model of the MAP two-year scanning strategy from G. Hinshaw (private communication), which gives the number of observations (N_{obs}) in each pixel at the end of the second year of the mission. The noise in each pixel is then $\propto N_{\text{obs}}^{-1/2}$. Fig. 10 shows the distribution of the r.m.s. noise distribution for MAP 90 GHz channel, with resolution ≥ 7 arcmin. In the figure, the noise average is $\langle r \rangle \simeq 97\mu\text{K}$ per pixel.

The effect of the inhomogeneous MAP noise can be incorporated into the formalism by defining the threshold level ν with respect to the noise level expected at each particular location, rather than with respect to the average r.m.s. noise level. The local noise can be inferred from the number of observations. In Fig. (11) we plot the effect of a inhomogeneous

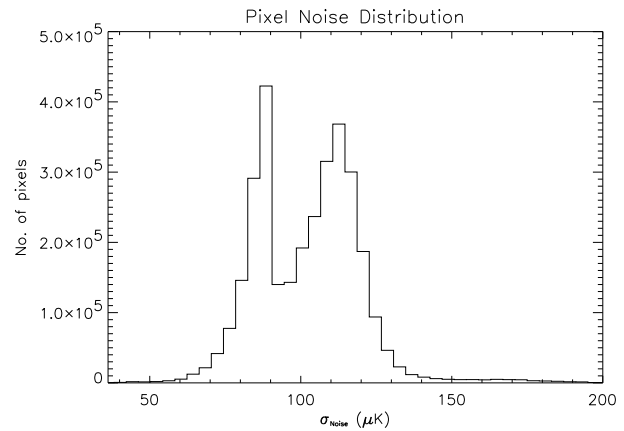


Fig. 10.— Histograms of pixel noise variance for the MAP 90 GHz channel with pixels size of 7 arcmins.

noise distribution in the raw estimate of $\xi_\nu(\theta)$. In this figure, the solid line represents the theoretical estimate obtained from eqs. (3) and (4). The dashed line represents the average obtained as discussed in Sec. 3.1. Both lines agree rather well up to $\theta \simeq 8^\circ$. For comparison we also plot ξ_ν for the case of homogeneous noise of Fig. (2).

4.2.3. Results

In the simulations we assumed that after foreground subtraction the foreground residuals would be about 10% and 20% the original amplitude at 90GHz. In the first case we selected a Galactic cut at $|b| = 5^\circ$ and 10° and for the 20% residuals we imposed a cut at $|b| = 20^\circ$. In all cases, we added inhomogeneous noise.

In Fig. (12) we show the results after including all the above terms. The results are shown for three different thresholds and for three different foreground residuals. The dotted line correspond to the input model. The solid line joins the average band power obtained from 200 simulations. The bandwidth is $\Delta l = 45$ and the error bars correspond to the 68% confidence level. Notice that that of temperature anisotropies be Gaussian, the inclusion of non-Gaussian effects from Galactic foregrounds has very little effect on the results. Our simulations show that the method gives almost identically accurate results for CMB power spectrum when the Galactic cut is lowered to $b_{\text{cut}} = 5^\circ$.

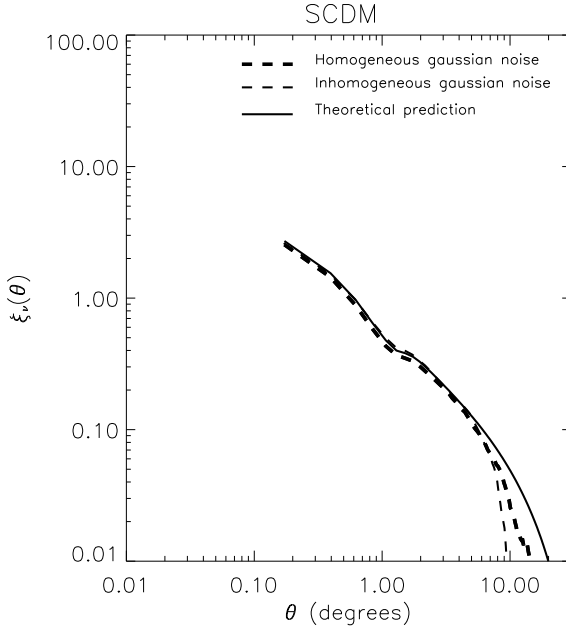


Fig. 11.— The 2-point correlation function ξ_ν with $\nu = 2$ for SCDM computed from a single realization of MAP 90GHz channel including an inhomogeneous noise distribution. Solid line corresponds to the input model, thin dashed line to ξ_2 from the data. For comparison, the fit to the data in the case of homogeneous noise of Fig. (2) is plotted as thick dashed line.

On the other hand, direct computation of the power spectrum from the map which necessarily has a cut due to bright foreground regions, is possible only with a finite band-width determined by size of the Galactic cut. This was avoided in the COBE DMR data with the Gramm-Schmidt orthogonalization of the base functions (Górski et al 1994), but the procedure is impractical for the mega-pixel CMB datasets. We note that the band-width over which we have to average in order to reach cosmic variance at the central l is a requirement shared with other methods. Our method recovers enough independent data points to trace the CMB spectrum with accuracy comparable to standard methods, but has a significant gain factor ($10^3 - 10^4$) in CPU time.

As demonstrated here the method works accurately in the presence of foregrounds and for the realistic/inhomogeneous MAP noise. The treatment in

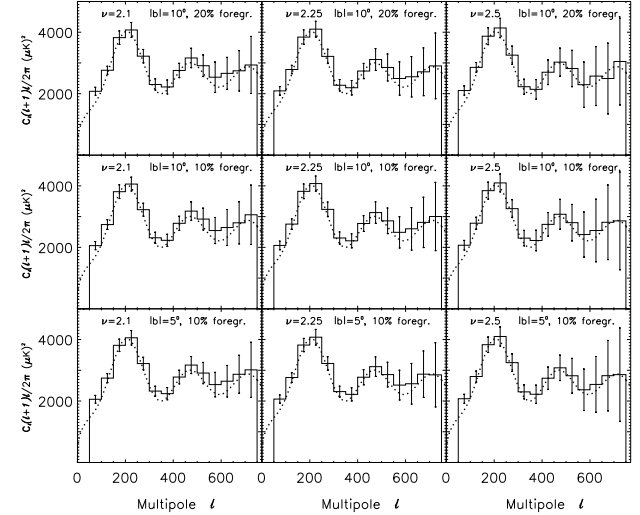


Fig. 12.— Radiation power spectra obtained from maps containing inhomogeneous noise and foreground residuals. In all plots, the dotted line corresponds to the input model, the solid line joins the average value of 500 simulations, error bars are 1σ errors.

the presence of the inhomogeneous noise can also be improved by removing the pixels with significantly fewer observations.

Finally we note that for the final MAP data the peaks method would work even more accurately, because one can combine various MAP channels and reduce the noise (and foregrounds) further. However, in that case the resolution would have to be downgraded to that of the lowest frequency channels.

Furthermore, because the peaks method computes a correlation function, ξ_ν , it is immune to masking. The latter would allow us to reduce the foregrounds signal by removing from the CMB maps more isolated regions with higher foreground contribution.

5. Application to Planck

The Planck satellite³ is due to be launched in early 2007 to map the all sky CMB distribution with an even finer resolution than MAP. It will have two in-

³(<http://astro.estec.esa.nl/Planck/>)

struments: the low-frequency instrument (LFI), that operates at four frequency channels between 30 and 100 GHz, and the high-frequency instrument (HFI) in six frequency channels between 100 and 857 GHz. The highest Planck resolution will be 5 arcmin and the instrument noise after one year of operations is expected to be around 6-10 μK . (For the 100 and 143 GHz channels with 10 and 8 arcmin resolution respectively, the noise is expected to be the smallest with the one-year rms of $\sim 5\mu\text{K}$).

For Planck we performed simulations with a homogeneous white noise. Due to the lack of proper templates for both Galactic emission and noise pattern in the sky, we did not include foregrounds in the analysis, but they are not expected to be important as demonstrated in Sec. 4. The simulations shown were performed for a (non-realistic) ΛCDM model with $\Omega_\Lambda = 0.3$ and $\Omega_{\text{CDM}} + \Omega_{\text{baryon}} = 0.7$. This model was chosen because it has prominent peak structure and to show that the KHA method recovers all of it very accurately.

We simulated the 217 GHz channel that has beam of 5.5° FWHM and the noise level of $11.4\mu\text{K}$ per beam area. The maximum multipole to which the beam is sensitive is $l_{\text{beam}} = 1472$. The HEALPix configuration chosen to pixelize the CMB sky as seen by this channel was $N_{\text{side}} = 1024$, which yields pixels of 3.5 arcmins. Due to PLANCK broad spectral coverage and the extremely low noise level of the 217GHz channel (almost negligible compared to the intrinsic CMB fluctuations at this angular scales) we expect that the effect of striping, inhomogeneous sky coverage and noise correlations will be irrelevant.

In Fig. (13) we show the results from 600 simulations. As in the MAP simulations, we chose three threshold levels that, on average, have twice the number of pixels that the next threshold. These thresholds have the same number of pixels as the corresponding simulations of MAP discussed previously. In the figure the band power is averaged in bins of $\Delta l = 45$. In Planck simulations we chose the thresholds with the same number of points (peaks) as in the MAP simulations and the method is able to recover the power spectrum out to $l = 1500$ with much higher accuracy. This means that our method reconstructs the power spectrum out to the highest multipole, determined by the beam, *irrespective* of the total number of peaks used in the analysis.

The band power error bars depend on the number of pixels (or the peak threshold ν) used in the calcula-

tion of the power spectrum and on the bandwidth Δl . In this case, a fit of the form $\sigma_{C_l} \propto N_{\text{peaks}}^\beta$ to the error bars of all multipoles gives: $\beta = -0.65 \pm 0.011$, close to the expected behavior $\sigma_{C_l} \propto 1/\sqrt{N_{\text{peaks}}}$. With respect to the bandwidth $\sigma_{C_l} \propto 1/\sqrt{\Delta l}$ for $\Delta l \gtrsim 10$, the scale where the correlation introduced by the Gaussian tapering is dominant.

6. Discussion and conclusions

We have presented the detailed implementation of the peaks KHA method for computing the CMB power spectrum. The method is based on the correlation properties of peaks on the CMB and assumes that temperature fluctuations are Gaussian. We have shown that for MAP and Planck datasets the method is robust in the presence of Galactic (non-Gaussian) foregrounds and realistic MAP noise inhomogeneities. Even without the bin-averaging the method determines the CMB power spectrum with uncertainty comparable to the cosmic variance. Because even with narrow band-width bin-averaging the CMB multipoles are sufficiently independent, the uncertainty can be decreased further with bin-averaging.

The method recovers enough independent values of the CMB multipoles to enable quick and accurate estimation of the cosmological parameters from MAP future data. For MAP the KHA method should work most optimally for peaks threshold of $\nu \sim 1.8 - 2.5$ or in only $(2.5 \times 10^{-3} - 8 \times 10^{-5})N^2$ operations.

Applying the method to the simulated PLANCK sky maps has shown that we could probe the power spectrum out to much higher multipoles and without loss of accuracy. For Planck mission parameters, the KHA method should work most optimally for peaks threshold of $\nu \sim 2 - 3$ reducing the number of step to only up to $\sim 4 \times 10^{-6}N^2$ operations for thresholds as high as $\nu \sim 3$. This can potentially lead to a gain of up to $\sim 10^5$ in speed compared to the existing $\mathcal{O}(N^2)$ methods.

Another advantage is that because we use a ξ_ν statistic the computed CMB spectrum is immune to masking allowing to remove high noise and foreground emission parts of the sky. Furthermore in this method we can select the accuracy of the final CMB spectrum by choosing the threshold accordingly.

With the scalings of σ_{C_l} with ν for both MAP and Planck one can estimate the uncertainties of the different multipoles at still lower peak threshold values. In Fig. (14) we show our projection for how accu-

rately the CMB power spectrum with lower threshold: $\nu = 2.1$ for Planck and $\nu = 1.6$ for MAP. The whole calculation would require only $\sim 6 \times 10^{-4} N^2$ and $6 \times 10^{-2} N^2$ operations.

Finally, it is illustrative to note that for the relevant parameters for the MAP and Planck datasets the KHA method performs even faster the direct $O(N^{1.61})$ computation. In Fig. (15) we plot the critical threshold ν at which the number of operations required by our method equals $N^{1.61}$. For comparison, for MAP parameters the method would work for $\nu \simeq (2 - 2.5)$ and for Planck it can work for ν as high as 3. In all cases the peaks method would be at least as fast, if not faster, than the $O(N^{1.61})$ computation, but at the same time it would be robust to Galactic and other cuts and noise inhomogeneities.

Acknowledgments We are particularly grateful to Gary Hinshaw for fruitful conversations and for providing us with the Galactic foregrounds model data and the MAP observations model used in the simulations. C.H.M. and F.A.B. acknowledge support of Junta de Castilla y León (project SA 19/00B) and Ministerio de Educación y Cultura (project BFM2000-1322). C.H.M. thanks the Astrophysikalisches Institut Potsdam for allowing him to use their computer resources.

REFERENCES

Bardeen, J.M., et al. 1986, Ap.J., 304, 15
 Bond, J.R., Jaffe, A.H. & Knox, L. 2000, Ap.J., 533, 19.
 Finkbeiner, D.P., Davis, M., Schlegel 1999, Ap.J., 524, 867
 Górski, K.M. 1994, Ap.J. 430, L85
 Górski, K.M., Hivon, E. & Wandelt, B.D. 1999 in Proc. MPA/ESO Conf. (eds. Banday, A.J., Sheth, R.K. & Da Costa, L.)
 Hinshaw, G. 2000, astro-ph/0011555
 Hivon, E., et al. 2002 Ap.J., 567, 2
 Hu, W. & Dodelson, S. 2002, A.R.A.A., in press. (astro-ph/0110414)
 Jensen, L.G. & Szalay, A.S. 1986 ApJ, 305, L5
 Kaiser, N. 1984 Ap.J., 282, L9
 Kashlinsky, A. 1987, Ap.J. 317, 19
 Kashlinsky, A., Hernández-Monteagudo, C. & Atrio-Barandela, F. (2001) Ap.J., 557, L1 (KHA)
 Kogut, A. et al. 1996, Ap.J., 464, L5
 Oh, S.P., Spergel, D.N. & Hinshaw, G. 1999 ApJ, 510, 551
 de Oliveira-Costa, A. et al. 1999, Ap.J., 527, L9
 Peebles, P.J.E. 1980 "The Large Scale Structure of

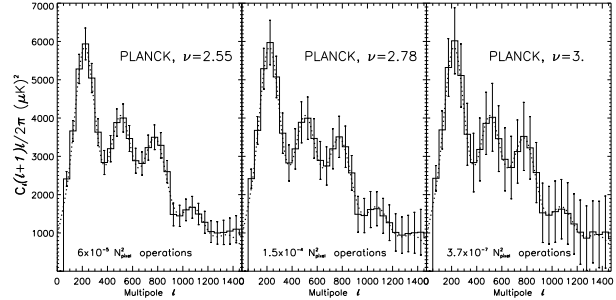


Fig. 13.— Radiation power spectrum for the 217 GHz channel. Dotted line is the input model, solid line the mean for 500 simulations, and error bars are at 1σ . The bandwidth is $\Delta l = 45$.

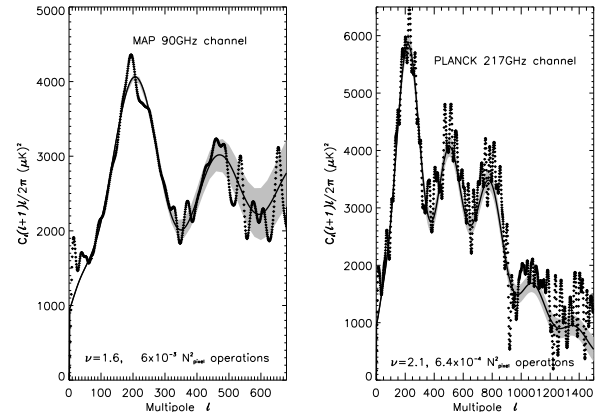


Fig. 14.— Radiation power spectrum that can be recovered from MAP data at $\nu = 1.6$ in only $6 \times 10^{-3} N^2$ operations and from Planck at $\nu = 2.1$ in $6 \times 10^{-4} N^2$ steps. The solid line corresponds to the input model and the dotted lines are the raw power spectrum result of one single simulation, prior to binning, as shown in top panels of Fig. (4). Shaded areas show the extrapolated 1-sigma uncertainties for determining the CMB power spectrum binned with $\Delta l = 45$.

the Universe”, Princeton University Press, Princeton Press, W.H. et al. 1992 “Numerical Recipes”, 2nd edition, Cambridge University Press, Cambridge
 Rice, S.O. 1954, in “Noise and Stochastic Processes”, ed. Wax, N., p.133 Dover (NY)
 Seljak, U. & Zaldarriaga, M. 1996, Ap. J., 469, 437
 Sokasian, A., Gawiser, E. & Smoot G.F. 1998, astro-ph/9811311.
 Szapudi, I. et al 2001a, Ap.J., 548, L115
 Szapudi, I., Prunet, S., Colombi, S. 2001b, Ap.J., 561, L11
 Schlegel, D.J., Finkbeiner, D.P., Davis, M. 1998, Ap.J., 500, 525
 Tegmark, M. 1997, Phys.Rev.D., 55, 5898
 Wandelt, B.D., Hivon, E. & Górski, K. 2001, Phys.Rev.D, 64, 083003

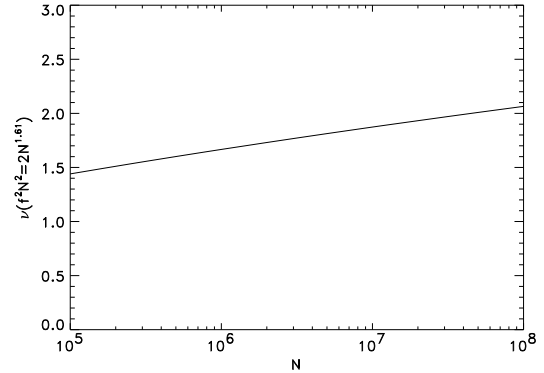


Fig. 15.— The value of the peak threshold where the number of operations in the KHA method equals $N^{1.61}$, is plotted as a function of the number of pixels.